Spectacular Oxygen Evolution Reaction Enhancement Through Laser Processing of the Nickel-Decorated Titania Nanotubes

Jakub Wawrzyniak, Jakub Karczewski, Emerson Coy, Igor Iatsunskyi, Jacek Ryl, Maria Gazda, Katarzyna Grochowska, Katarzyna Siuzdak*

J. Wawrzyniak, Dr. K. Grochowska, Prof. K. Siuzdak,
Centre for Plasma and Laser Engineering
The Szewalski Institute of Fluid-Flow Machinery, Polish Academy of Sciences, Fiszera 14 st., 80-231 Gdańsk, Poland
E-mail: jwawrzyniak@imp.gda.pl

Dr. J. Karczewski, Prof. M. Gazda
Department of Solid-State Physics
Gdańsk University of Technology, Gabriela Narutowicza 11/12 st., 80-233 Gdańsk, Poland

Prof. E. Coy, Prof. I. Iatsunskyi
NanoBioMedical Centre
Adam Mickiewicz University, Wszechnicy Piastowkiej 3 st., 61-614 Poznań, Poland

Prof. J. Ryl
Department of Electrochemistry, Corrosion and Materials Engineering
Gdańsk University of Technology, Gabriela Narutowicza 11/12 st., 80-233 Gdańsk, Poland

Keywords: titania nanotubes, laser treatment, water splitting, nickel

The selective, laser-induced modification of the nickel-decorated titania nanotubes provides remarkable enhancement towards oxygen evolution reaction. Particularly, the irradiation of the laterally spaced crystalline TiO_2 nanotubes, results in the formation of the tight closure over irradiated end, preserving their hollow interior. The shape of the absorbance spectra is modulated along with applied energy, and the new absorption band appears at 500 nm, where the local minimum can be found for bare nanotubes. The high-resolution X-ray photoelectron spectra indicate the presence of both metallic and hydroxide forms of nickel species. The electrode material treated with 355 nm pulses at 50 mJ cm^{-2} shows significantly improved current densities in the anodic regime, reaching nearly 300 mA cm^{-2} while exposed to solar radiation, whereas the untreated sample barely comes to 1.5 mA cm^{-2} in the same conditions. The tailored titania photoanode also exhibits two orders of magnitude higher donor concentration in comparison to the primary substrate as verified by Mott-Schottky analysis. The electrochemical analysis confirms the key role of laser annealing in enhancing the effectiveness of light-driven water splitting.

1. Introduction

Growing concerns for a natural environment drive innovation towards novel, clean energy sources and storage devices.[1,2] Among them, cheap but efficient water-splitting devices are being developed, and great hopes are being put into light-enabled catalysts. The titania-based electrode materials are especially looked at, because of their abundance, flexibility, and high stability within a wide pH range.[3] Moreover, there are plentiful forms in which titania can be synthesized, which makes it a perfect target for further modifications. Apart from decoration with foreign species, doping, and formation of non-stoichiometric titania,[4–9] many works rely upon the manipulation of titania architecture to improve its light-harvesting capabilities.[10,11] The ordered titania nanotubes (TiO_2NTs) are of particular interest, due to the straight charge percolation path, high surface area, and adjustable geometrical features. The optimized electrochemical oxidation of the titanium sheet provides control over the length,[12] diameter,[13,14] and spacing[15,16] of the nanotubes, which allows their tailoring towards specific applications. Adjustments of the surface morphology do not stop with an anodization process, though. With the additional post-processing such as flame annealing,[17] atomic layer deposition,[18] or plasma treatment,[19] crystallinity, and photoelectrochemical response can be freely adjusted as well. Considering efficient water splitting, catalysts containing abundant transition metals are recently being explored,[20] but often require laborious techniques and generate a lot of harmful waste. Regardless of the treatment procedure, the electrochemical performance of the modified substrate does not exceed a several-fold increase in comparison to the original material.[21,22] In this paper, spectacular oxygen evolution reaction (OER) and photoresponse improvements of the nickel-decorated titania nanotubes are reported. Incorporation of the 355 nm pulsed laser irradiation, as well as the use of titanium and nickel in their pure metallic forms, minimizes the generation of chemical waste. Moreover, the proposed processing technique can be applied onto a platform of any dimension, as each step of the synthesis is highly scalable.[23,24]

2. Results and discussion

2.1. Physical Characteristics

SEM images of laterally spaced TiO_2 nanotubes before and after modifications as well as TEM pictures of the single closed nanotube are shown in **Figure 1**. The as-prepared nanotubes can be characterized by the outer diameter of 188 ± 31 nm, an inner diameter of 142 ± 35 nm, the distance between their centers of 300 ± 70 nm, and length of 1.5 ± 0.1 μm.

Although the deposition of 5 nm thick Ni layer does not affect overall geometry, it is visible as the rim over the NT openings. Mild laser irradiation (10 mJ cm^{-2}) leads to the slight deformation of the top nanotube regime not noticeably affecting their length. For 20 mJ cm^{-2}, the length of the NTs drops to 1.1 ± 0.2 µm, but the selective closing of NTs is more pronounced. Laser treatment with 30 mJ cm^{-2} results in complete sealing of the nanotubes, while further increase in laser energy causes the coupling of the neighboring nanotubes through bridge-like structures (**Figure S1**). Nevertheless, throughout the modification process, the interior of the nanotubes remains intact. The EDX and SAED investigation of the sealed cap revealed mostly anatase phase with metallic nickel and NiO concentrated within the melted region (**Figure S2**). To confirm the presence of the crystalline phase of TiO_2 and Ni/NiO species, XRD patterns were recorded in θ–θ geometry and grazing incidence (**Figure S3)**. Pristine TiO_2 nanotubes reveal reflections at 25.3°, 37.2°, 38.1°, 48°, and 55.03° which corresponds with anatase, while at 35.2°, 38.5°, 40.2°, 53.1°, 63°, 70.7°, 76.4°, and 82.3° (weak) with Ti.[25,26] Additional, very faint signal at 27.5°, 37.1°, and 54.2° can be ascribed to residual quantities of rutile phase, as the formation of the rutile oxide layer is initiated at the Ti/TiO_2NTs interface.[27] The grazing-incidence XRD reveals more intense rutile peaks at higher angles, indicating its majority share in lower parts of the NTs. High-resolution XPS spectra show signals typical for Ti^{4+} and oxygen attributed to the lattice Ti-O and surface Ti-OH,[28] whereas C1s signal can be assigned to adventitious carbon as typical contamination originating from the instrument and organic residues from the anodization bath (**Figure S4**).[29] Moreover fitting the peaks at 852.6 eV (spin-energy separation of 19.4 eV) and 855.8 eV (spin-energy separation 17.7 eV) confirms the presence of metallic and hydroxide $Ni(OH)_2$ forms of nickel respectively.[30–32] While Ni 2p3/2 peak location and geometry confirms the dominant contribution from $Ni(OH)_2$, the surface contribution of NiOOH or even NiO cannot be completely neglected (**Figure 2a**). Furthermore, the optical properties of the NTs were analyzed based on the UV-Vis measurements (**Figure 2b**). The pristine TiO_2 nanotubes show typical, strong UV absorption, while the deposition of nickel results in an increase of absorbance in the visible range, as well as the formation of the interference fringes.[28,33] Moreover, the red-shifted band edge is observed, likely due to the decrease of the energy gap between Ti (d) and O (p) orbitals.[34] Mild irradiation leads to a further increase of absorption in the visible range, while higher reflection in UV is observed, resulting in a similar level of absorbance over the whole spectrum. At higher investigated fluences, more visible than UV light is being absorbed. It can be explained by the formation of the caps over the NTs which may partly reflect incident radiation, or by the elevated number of oxygen vacancies created by the laser.[35] From the reflectance spectra, the Kubelka-Munk plots were calculated (**Figure S5**), and the energy bandgap (E_{bg}) values were estimated for reference, nickel sputtered sample, and specimen irradiated with 10 mJ cm^{-2}. The E_{bg} of pristine titania NTs equals 3.09 eV, less than reported for bulk anatase (3.20 eV),[36] due to optimization of the spacing and geometrical features of the nanotubes.[37] As expected, the E_{bg} values drop to 3.00 eV for Ni-decorated sample, and further to 2.88 eV after irradiating with 10 mJ cm^{-2}. A similar trend was observed previously for laser-treated Cu-TiO_2 NTs,[38] which indicates synergistic effects of metal/metal oxide and laser processing in E_{bg} reduction. In the case of higher laser fluences, it was impossible to derive optical bandgap values, due to the leveled character of absorbance spectra over the measured range.

2.2. Electrochemical performance

Figure 3a shows linear voltammetry diagrams measured in the dark and under AM 1.5 illumination. At the highest investigated potential (2.6 V vs RHE), the current density of the reference sample can be seen at 1 mA cm^{-2}, while the magnetron-sputtered sample exhibits currents 60% higher. The laser-modified specimens, however, dwarfs the reference sample as their current densities exhibit values 14 to 240 times greater in the dark, and up to 280 times higher under applied AM 1.5 radiation. The enhancements of the current densities scale along the laser fluence applied during modification, although the factor of improvement is much greater. In the dark, modification with 10 mJ cm^{-2} boosts performance by only about 14 times, whereas applying 20 mJ cm^{-2} accounts for 145 times higher currents. In the case of the highest investigated fluence (50 mJ cm^{-2}), the current density of 240 mA cm^{-2} was measured. Additional investigation under solar spectrum shows, that the obtained material exhibits photoactive properties, as the current densities rose by up to 50% for sample modified with 10 mJ cm^{-2} and by ca. 17% for those treated with higher energy laser pulses. The linear voltammetric sweeps also reveal oxidation from NiO to NiOOH at 1.45 V (**Figure S6**),[39] and passivation of surface species or defects at ca. 2 V.[40] The overpotential η for oxygen evolution reaction is shown for 10 mA cm^{-2},[41] and shifts towards lower values when higher the laser fluence is applied - this trend is further reinforced under the exposure to solar light. Interestingly, the biggest difference is observed between Ni-decorated but untreated sample, which never passes the desired current, the one modified with 10 mJ cm^{-2}, which reaches 10 mA cm^{-2} at η = 1.07 V, and the sample irradiated with 20 mJ cm^{-2} laser pulses, which crosses it at η = 0.57 V. Further increases in lasing energy, however, accounts only for an additional decrease of 150 mV, down to η = 420 mV. For the samples reaching 10 mA cm^{-2} the Tafel slopes have been calculated and shown in **Figure 3b**. It can be seen, that the initially steep slope of the sample irradiated with 10 mJ cm^{-}

^{2} flattens above 20 mJ cm^{-2}. The graph shows that the sample irradiated with 50 mJ cm^{-2} has the mildest slope, indicating the fastest OER kinetics. The density of charge carriers (N_d) was calculated from the Mott-Schottky diagram (**Figure 3c**),[42,43] and two orders of magnitude difference is observed between the reference (6.69×10^{19} cm^{-3}) and the best performing laser-treated sample (4.09×10^{21} cm^{-3}). The flatband potential was lowered from 0.34 V in the bare substrate to 0.28 V for the most active modified titania. Although the same amount of nickel is present in every case (aside from reference), the results vary drastically. It evidences, that the laser-irradiation plays a crucial role in the reordering of the atoms in the modified region and creating surface states that improve OER kinetics, despite the overall loss of the surface area as shown by the SEM investigation (Figure 1). Moreover, the material is very stable under galvanostatic load (10 mA cm^{-2}), as less than 1% change in the potential was observed during a 12-hour long load (**Figure 3d**). Overall, the obtained overpotential values and current densities situate the presented material among the best electrodes for oxygen production (**Table S8**). **Figure 3e** presents the Nyquist impedance plots of the highest-performing and reference samples, whereas plots of the remaining specimen are presented in **Figure S7**. The obtained spectra have been fitted using an electric equivalent circuit (EQC) formerly proposed by Bredar and Klahr[44,45] with χ^2 of the order of 10^{-3} – 10^{-5}. It contains three resistors (R), two constant phase elements (CPE), and an open Warburg diffusion (W_o), which values are shown in **Table S9**. Due to the inherently irregular NTs surface, the CPE is characterized by the $Z = Q^{-1}(i\omega)^{-n}$ where frequency dispersion n is taken into account.[46] While the low R_e stands for the electrolyte resistance, the R_1CPE_1 and R_2CPE_2 represent double-layer capacitance of porous bulk in the high, and surface states in the low-frequency range. The comparison between reference and laser-annealed materials reveals lower R_1 and CPE_1 due to increased donor concentration (Fig. 3b) and lower available surface area resulting from laser-induced sealing (Fig. 1c). The increased CPE_2 indicates a higher double-layer capacitance of defect states located on the material/electrolyte interface which are crucial for OER.[44] The finite-length ion diffusion with a reflective boundary can be described via W_o, where:

$$Z_{W_o}(\omega) = \frac{W_{or}}{\sqrt{\omega}}(1-j)\,coth(W_{oc}\sqrt{j\omega})$$

The W_{or} is a Warburg coefficient, and $W_{oc} = d/D^{0.5}$ where d is a length of Nerstian diffusion, and D is a diffusion coefficient of the electroactive species. The lower W_o relates to the charge transport within the NT walls to the blocking electrode. In both cases, the light-induced excitons contribute to the lowering of the electrode resistance.

3. Conclusion

Utilization of the precise laser processing of the nickel-coated nanotubes allows for a quick formation of closed, self-standing nanopillars with greatly enhanced photocatalytic properties. Due to the synergistic effect of nickel decoration and laser irradiation, the UV-vis spectra exhibits an additional absorbance band between 400 and 600 nm and the donor concentration increases by two orders of magnitude. The series of modified titania samples were electrochemically tested towards OER in the dark and under simulated solar irradiance allowing to track the influence of both Ni and laser within 10-50 mJ cm^{-2} range. Most notably, the modification at 50 mJ cm^{-2} enables generation of nearly 300 mA cm^{-2} at ca. 2.6 V vs RHE, which stands in stark contrast with nanotubes that were not irradiated and barely reached 1.5 mA cm^{-2} in the same conditions. Moreover, the exceptional stability of the sample was observed, as the galvanostatic evaluation reveals over 99% potential retention after a 12-hour working period. To the best of our knowledge, this is the first time such an approach was used to develop highly efficient, yet very stable photoanode material for OER in alkaline media.

4. Experimental Section

Material synthesis: The titania nanotubes were created via electrochemical anodization in the two-electrode system. The degreased titanium foil acting as an anode was immersed in diethylene glycol-based electrolyte, containing 0.3 wt% NH_4F, 0.5 wt% HF, and 7 wt% deionized water. The process was conducted at 40 V under a controlled temperature of 40°C for 2h. After anodization, the foil was rinsed with ethanol and dried in air. To obtain the reference, anatase TiO_2, the samples were calcined in a furnace at 450°C for 2h. The samples were then decorated with 5 nm of nickel via magnetron sputtering using Ni target (99.99 %) and placed onto the motorized table in the vacuum chamber (5×10^{-5} mbar). They underwent laser treatment with Nd:YAG pulsed laser equipped with 3rd harmonics generator and beam homogenizer within 0 – 50 mJ cm^{-2} fluence range. *Characterization:* SEM images were taken with FE-SEM FEI Quanta FEG 250 while TEM investigation was done using JEOL ARM 200F. XRD patterns were recorded by Bruker D2Phaser diffractometer with Cu Kα radiation over 20 – 90° range, while the grazing incidence XRD patterns were obtained via Philips X'Pert MPD diffractometer with Cu Kα radiation over 20 – 40° range and incidence angle between 1 and 4°. The XPS spectra were obtained from sample treated with 50 mJ cm^{-2} via Escalab250Xi calibrated for adventitious C1s (284.6 eV),[47] using Al Kα anode. Optical reflectance spectra were obtained by the PerkinElmer dual-beam spectrophotometer at a scanning speed of 120 nm min^{-1}. The electrochemical properties were studied in deaerated 0.5 M NaOH with Autolab PGStat 302 N in a three-electrode system, where the prepared sample acted as a working electrode, while platinum mesh and Ag/AgCl/0.1 M KCl were used as a counter- and reference electrodes respectively. The potential values were recalculated towards RHE using following relation: $E_{RHE} = E_{Ag/AgCl/0.1\ M\ KCl} + E^0_{Ag/AgCl/0.1\ M\ KCl} + 0.059\ \text{pH}$ where $E^0_{Ag/AgCl/0.1\ M\ KCl} = 0.288$ V and pH = 13.69 for 0.5 M NaOH solution. Cyclic voltammetry sweeps (0.1 – 2.6 V vs RHE, 50 mV s^{-1}) in the dark and under the illumination of a solar simulator (Oriel LS0500, AM 1.5) preceded linear voltammetry scans (0.1 – 2.6 V vs RHE, 10 mV s^{-1}) to reach the chemical equilibrium of the working electrode. The impedance measurements were performed at the open circuit potential (OCP) in 20000 – 0.1 Hz range at 20 points per decade, whereas the Mott-Schottky analysis was carried out based on the data from potentiodynamic electrochemical impedance spectroscopy carried out between -0.1 and 1.9 V vs RHE at 1 kHz, at the 10 mV amplitude. The spectra were fitted with EIS Analyser[48] using Powell algorithm. All of the chemicals used are considered pure for analysis. For a more detailed description of the NT synthesis, please refer to our previous work.[37]

Acknowledgments

This work received financial support from the Polish National Science Centre: Grant No. 2017/26/E/ST5/00416. E.C and I.I acknowledge the partial financial support under the grant (UMO-2019/35/B/ST5/00248).

References

[1] M. M. Tavakoli, G. Azzellino, M. Hempel, A. Lu, F. J. Martin-Martinez, J. Zhao, J. Yeo, T. Palacios, M. J. Buehler, Adv. Funct. Mater., 2020, 2001924. https://doi.org/10.1002/adfm.202001924.

[2] M. Dehghanimadvar, R. Shirmohammadi, M. Sadeghzadeh, A. Aslani, R. Ghasempour, Int. J. Energy Res., 2020, 1. https://doi.org/10.1002/er.5508.

[3] V. Mahajan, S. Mohapatra, M. Misra, Int. J. Hydrogen Energy, 2008, 33, 5369. https://doi.org/10.1016/j.ijhydene.2008.06.074.

[4] C. Xu, Y. Song, L. Lu, C. Cheng, D. Liu, X. Fang, X. Chen, X. Zhu, D. Li, Nanoscale Res. Lett., 2013, 8, 391. https://doi.org/10.1186/1556-276X-8-391.

[5] M. Nasirian, Y. P. Lin, C. F. Bustillo-Lecompte, M. Mehrvar, Int. J. Environ. Sci. Technol., 2018, 15, 2009. https://doi.org/10.1007/s13762-017-1618-2.

[6] R. P. Vitiello, J. M. Macak, A. Ghicov, H. Tsuchiya, L. F. P. Dick, P. Schmuki, Electrochem. Commun., 2006, 8, 544. https://doi.org/10.1016/j.elecom.2006.01.023.

[7] L. Sun, J. Li, C. L. Wang, S. F. Li, H. B. Chen, C. J. Lin, Sol. Energy Mater. Sol. Cells, 2009, 93, 1875–1880. https://doi.org/10.1016/j.solmat.2009.07.001.

[8] M. N. Shaddad, D. Cardenas-Morcoso, M. García-Tecedor, F. Fabregat-Santiago, J. Bisquert, A. M. Al-Mayouf, S. Gimenez, ACS Omega, 2019, 4, 16095. https://doi.org/10.1021/acsomega.9b02297.

[9] A. Kertmen, E. Barbé, M. Szkoda, K. Siuzdak, V. Babačić, P. Torruella, I. Iatsunskyi, M. Kotkowiak, K. Rytel, S. Estradé, F. Peiró, S. Jurga, Y. Li, E. Coy, Adv. Mater. Interfaces, 2018, 1801286. https://doi.org/10.1002/admi.201801286.

[10] R. Qu, N. Liu, Y. Chen, W. Zhang, G. Zhu, Q. Zhang, L. Feng, Adv. Mater. Technol., 2017, 2, 1700125. https://doi.org/10.1002/admt.201700125.

[11] X. Wang, Z. Li, J. Shi, Y. Yu, Chem. Rev., 2014, 114, 9346. https://doi.org/10.1021/cr400633s.

[12] M. Paulose, H. E. Prakasam, O. K. Varghese, L. Peng, K. C. Popat, G. K. Mor, T. A. Desai, C. A. Grimes, J. Phys. Chem. C, 2007, 111, 14992. https://doi.org/10.1021/jp075258r.

[13] X. Wang, L. Sun, S. Zhang, X. Wang, ACS Appl. Mater. Interfaces, 2014, 6, 1361. https://doi.org/10.1021/am404966e.

[14] A. Mohammadpour K. Shankar, J. Mater. Chem., 2010, 20, 8474. https://doi.org/10.1039/c0jm02198a.

[15] F. Riboni, N. T. Nguyen, S. So, P. Schmuki, Nanoscale Horiz., 2016, 1, 445. https://doi.org/10.1039/C6NH00054A.

[16] N. T. Nguyen, S. Ozkan, I. Hwang, A. Mazare, P. Schmuki, Nanoscale, 2016, 8, 16868. https://doi.org/10.1039/C6NR06329B.

[17] A. Mazare, I. Paramasivam, F. Schmidt-Stein, K. Lee, I. Demetrescu, P. Schmuki, Electrochim. Acta, 2012, 66, 12. https://doi.org/10.1016/j.electacta.2012.01.001.

[18] F. Dvorak, R. Zazpe, M. Krbal, H. Sopha, J. Prikryl, S. Ng, L. Hromadko, F. Bures, J. M. Macak, Appl. Mater. Today, 2019, 14, 1. https://doi.org/10.1016/j.apmt.2018.11.005.

[19] T. Zhang, S. Cui, B. Yu, Z. Liu, D. Wang, Chem. Comm., 2015, 51, 16940. https://doi.org/10.1039/C5CC06454F.

[20] F. Lyu, Q. Wang, S. M. Choi, Y. Yin, Small, 2019, 15, 1804201. https://doi.org/10.1002/smll.201804201.

[21] C. E. Finke, S. T. Omelchenko, J. T. Jasper, M. F. Lichterman, C. G. Read, N. S. Lewis, M. R. Hoffmann, Energy Environ. Sci. 2019, 12, 358. https://doi.org/10.1039/C8EE02351D.

[22] Y. Hu, T. Ding, K. Zhang, B. Li, B. Zhu, K. Tang, ChemNanoMat, 2018, 4, 1133. https://doi.org/10.1002/cnma.201800252.

[23] C. Xiang, L. Sun, Y. Wang, G. Wang, X. Zhao, S. Zhang, J. Phys. Chem. C, 2017, 121, 15448. https://doi.org/10.1021/acs.jpcc.7b03124.

[24] L. Assaud, S. Bochmann, S. Christiansen, J. Bachmann, Rev. Sci. Instrum., 2015, 86, 073902. https://doi.org/10.1063/1.4926746.

[25] S. Meriam Suhaimy, C. Lai, H. Tajuddin, E. Samsudin, M. Johan, Materials, 2018, 11, 2066. https://doi.org/10.3390/ma11112066.

[26] D. Gu, Y. Wang, Z. Li, Y. Liu, B. Wang, H. Wu, RSC Adv., 2016, 6, 63711. https://doi.org/10.1039/C6RA12031H.

[27] S. Das, R. Zazpe, J. Prikryl, P. Knotek, M. Krbal, H. Sopha, V. Podzemna, J. M. Macak, Electrochim. Acta, 2016, 213, 452. https://doi.org/10.1016/j.electacta.2016.07.135.

[28] Ł. Haryński, K. Grochowska, J. Karczewski, J. Ryl, K. Siuzdak, ACS Appl. Mater. Interfaces, 2020, 12, 3225. https://doi.org/10.1021/acsami.9b19206.

[29] K. Siuzdak, M. Szkoda, A. Lisowska-Oleksiak, K. Grochowska, J. Karczewski, J. Ryl, Appl. Surf. Sci., 2015, 357, 942. https://doi.org/10.1016/j.apsusc.2015.09.130.

[30] H. W. Nesbitt, D. Legrand, G. M. Bancroft, Phys. Chem. Miner. 2000, 27, 357. https://doi.org/10.1007/s002690050265.

[31] Z. Zhang, Y. Jiang, X. Zheng, X. Sun, Y. Guo, New J. Chem., 2018, 42, 11285. https://doi.org/10.1039/C8NJ01910J.

[32] A. P. Grosvenor, M. C. Biesinger, R. St. C. Smart, N. S. McIntyre, Surf. Sci., 2006, 600, 1771. https://doi.org/10.1016/j.susc.2006.01.041.

[33] G. L. Chiarello, A. Zuliani, D. Ceresoli, R. Martinazzo, E. Selli, ACS Catal., 2016, 6, 1345. https://doi.org/10.1021/acscatal.5b02817.

[34] Z. Wu, Y. Wang, L. Sun, Y. Mao, M. Wang, C. Lin, J. Mater. Chem. A, 2014, 2, 8223. https://doi.org/10.1039/c4ta00850b.

[35] J. V. Pasikhani, N. Gilani, A. E. Pirbazari, Solid State Sci., 2018, 84, 57. https://doi.org/10.1016/j.solidstatesciences.2018.08.003.

[36] C. Dette, M. A. Pérez-Osorio, C. S. Kley, P. Punke, C. E. Patrick, P. Jacobson, F. Giustino, S. J. Jung, K. Kern, Nano Lett., 2014, 14, 11, 6533. https://doi.org/10.1021/nl503131s.

[37] J. Wawrzyniak, K. Grochowska, J. Karczewski, P. Kupracz, J. Ryl, A. Dołęga, K. Siuzdak, Surf. Coat. Technol., 2020, 389, 125628. https://doi.org/10.1016/j.surfcoat.2020.125628.

[38] K. Grochowska, Z. Molenda, J. Karczewski, J. Bachmann, K. Darowicki, J. Ryl, K. Siuzdak, Int. J. Hydrogen Energy, 2020. https://doi.org/10.1016/j.ijhydene.2020.05.054.

[39] M. Yang, L. Huo, L. Pei, K. Pan, Y. Gan, Electrochim. Acta, 2014, 125, 288. https://doi.org/10.1016/j.electacta.2014.01.109.

[40] A. Mazare, M. Dilea, D. Ionita, I. Demetrescu, Surf. Interface Anal., 2014, 46, 186–192. https://doi.org/10.1002/sia.5364.

[41] Y. Yin, X. Zhang, C. Sun, Prog. Nat. Sci.: Mater. Int., 2018, 28, 430. https://doi.org/10.1016/j.pnsc.2018.07.005.

[42] R. Beranek, Adv. Phys. Chem., 2011, 2011, 1. https://doi.org/10.1155/2011/786759.

[43] H. Tsuchiya, J. M. Macak, A. Ghicov, A. S. Räder, L. Taveira, P. Schmuki, Corros. Sci., 2007, 49, 203. https://doi.org/10.1016/j.corsci.2006.05.009.

[44] A. R. C. Bredar, A. L. Chown, A. R. Burton, B. H. Farnum, ACS Appl. Energy Mater., 2020, 3, 66. https://doi.org/10.1021/acsaem.9b01965.

[45] B. Klahr, S. Gimenez, F. Fabregat-Santiago, T. Hamann, J. Bisquert, J. Am. Chem. Soc., 2012, 134, 4294. https://doi.org/10.1021/ja210755h.

[46] G. J. Brug, A. L. G. van den Eeden, M. Sluyters-Rehbach, J. H. Sluyters, J. Electroanal. Chem. Interfacial Electrochem., 1984, 176, 275. https://doi.org/10.1016/S0022-0728(84)80324-1.

[47] P. Swift, Surf. Interface Anal., 1982, 4, 47. https://doi.org/10.1002/sia.740040204.

[48] G. A. Ragoisha, A. S. Bondarenko, Electrochim. Acta, 2005, 50, 1553. https://doi.org/10.1016/j.electacta.2004.10.055.

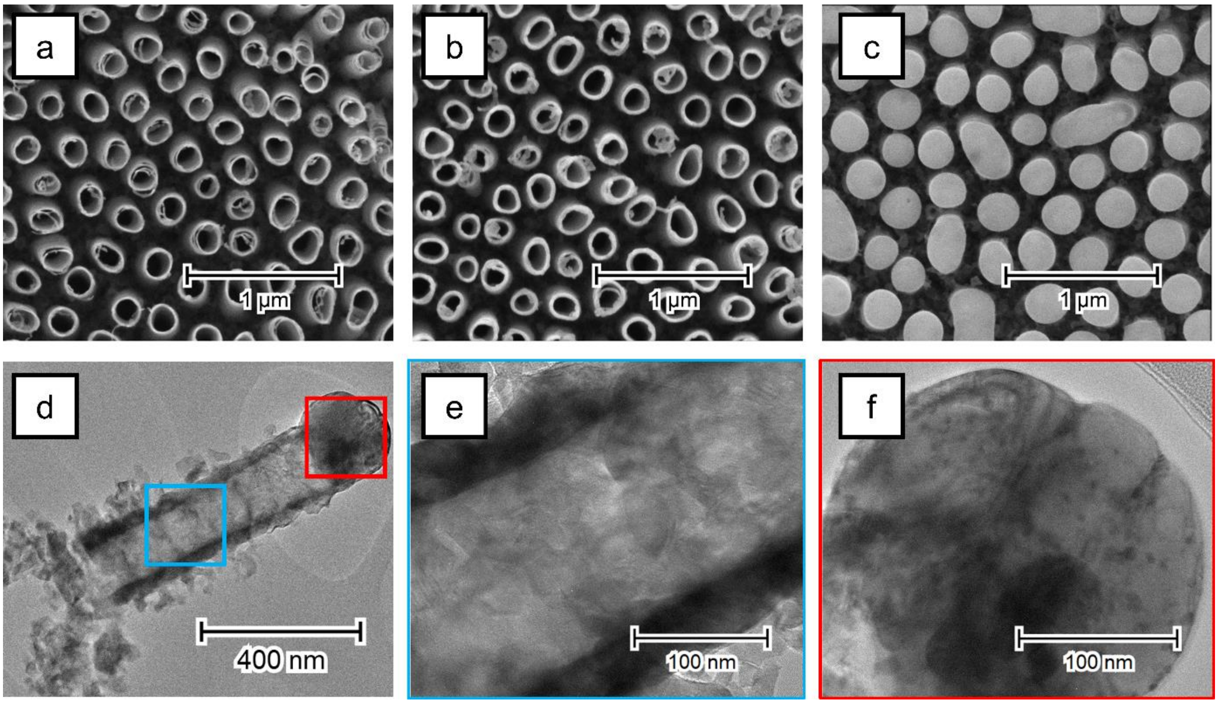

Figure 1: SEM images of the as-anodized titania nanotubes (a), the NTs after sputtering with 5nm nickel (b), and after laser-treatment with 50 mJ cm^{-2} (c). TEM image of a single nanotube (d), close-up of its core (e), and its cap (f).

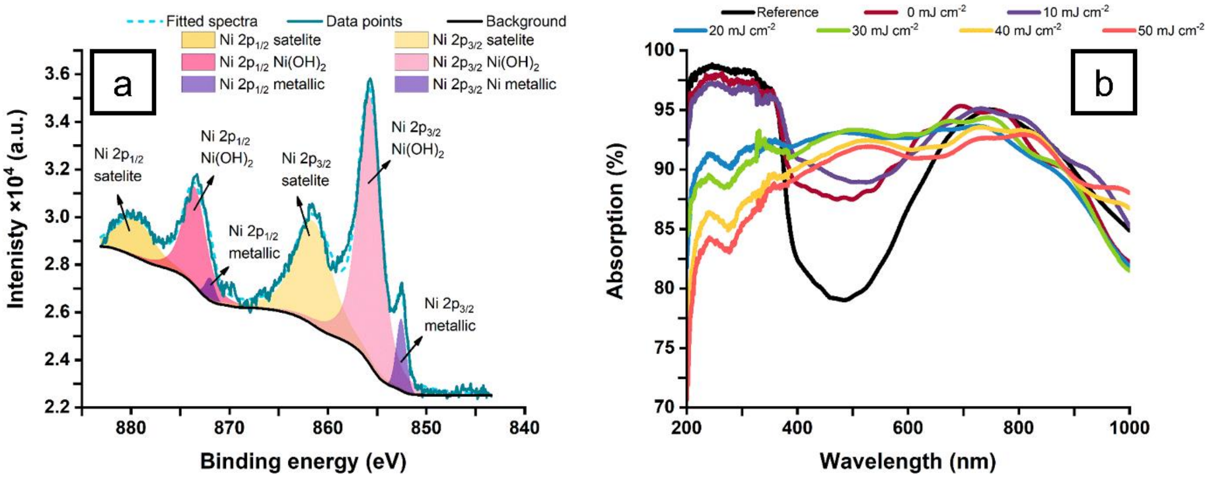

Figure 2: Deconvoluted XPS spectra of Ni (a). UV-vis absorbance spectra of reference and laser-modified samples (b).

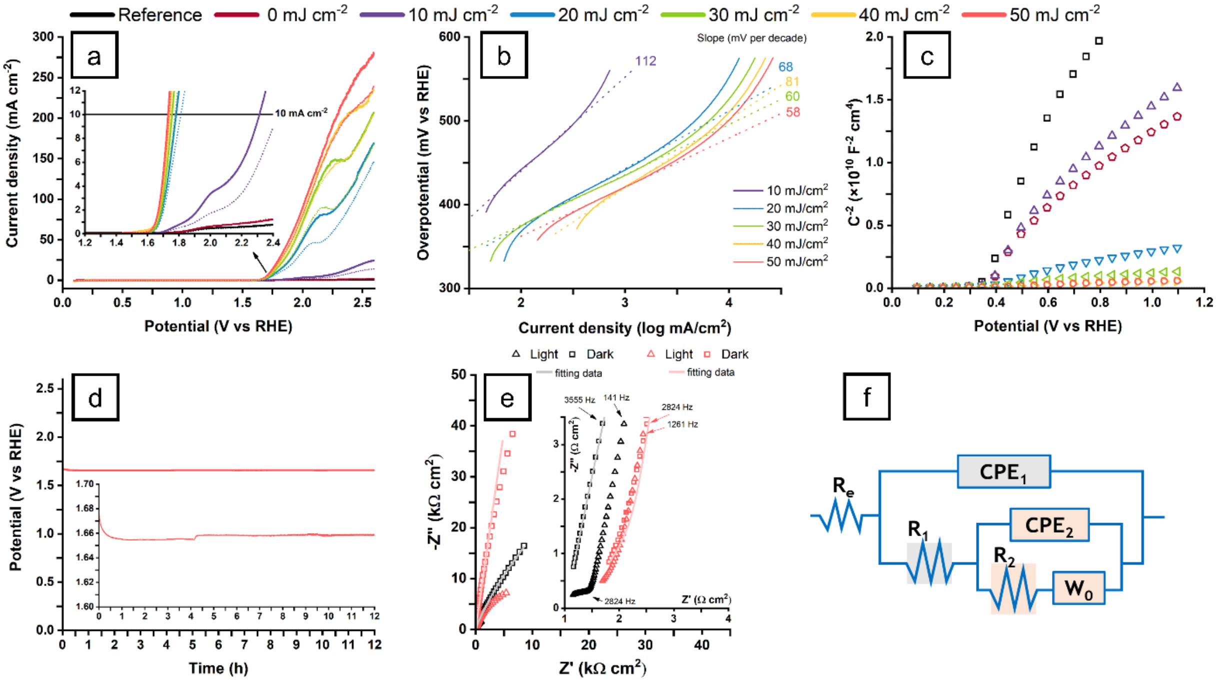

Figure 3: Chemical analysis of the reference and laser-modified samples. Linear voltammogram (a), Tafel plot (b), Mott-Schottky plot (c), galvanostatic load at 10 mA cm^{-2} (d), Nyquist representation of the impedance spectra for best and reference sample (e), electric equivalent circuit used for fitting (f)

Supporting Information

Spectacular Oxygen Evolution Reaction Enhancement Through Laser Processing of the Nickel-Decorated Titania Nanotubes

Jakub Wawrzyniak, Jakub Karczewski, Emerson Coy, Igor Iatsunskyi, Jacek Ryl, Maria Gazda, Katarzyna Grochowska, Katarzyna Siuzdak*

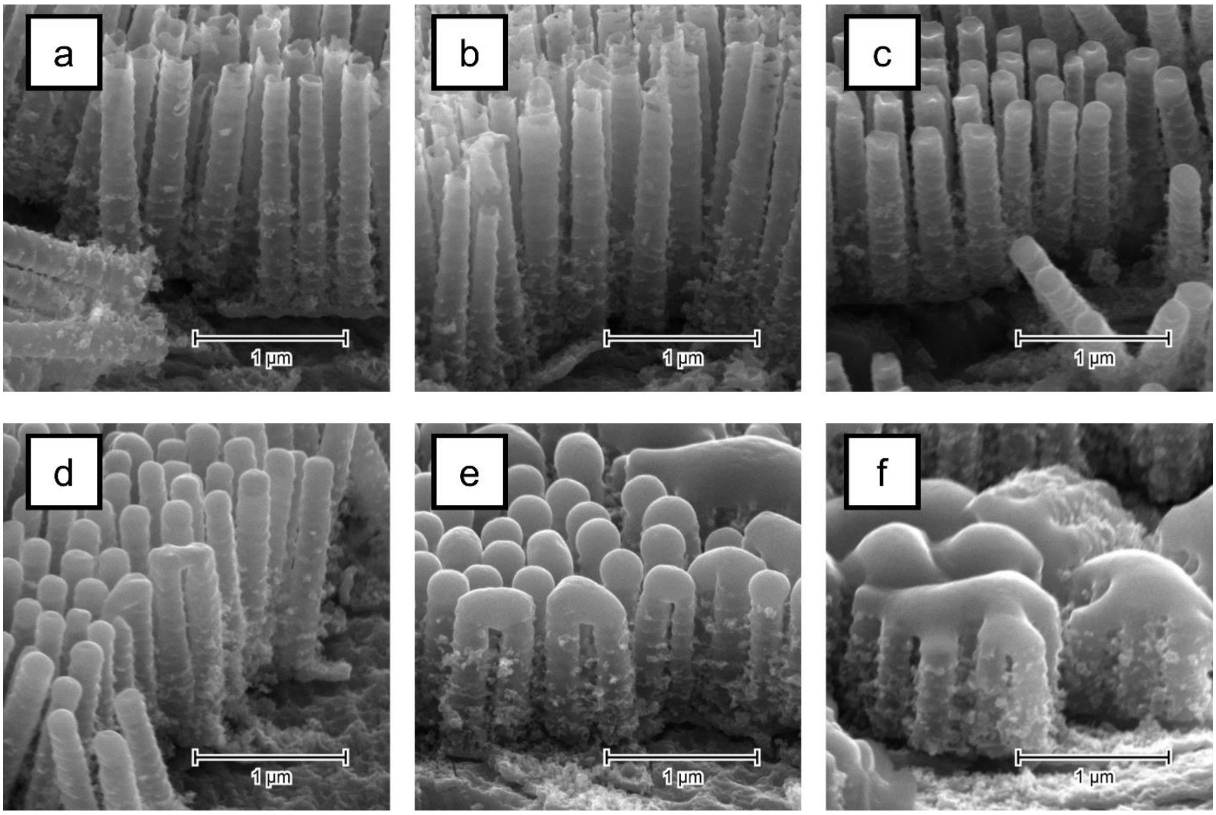

Figure S1: SEM images of the cross-section of the samples irradiated with 0 (a) – 50 (f) mJ cm^{-2}.

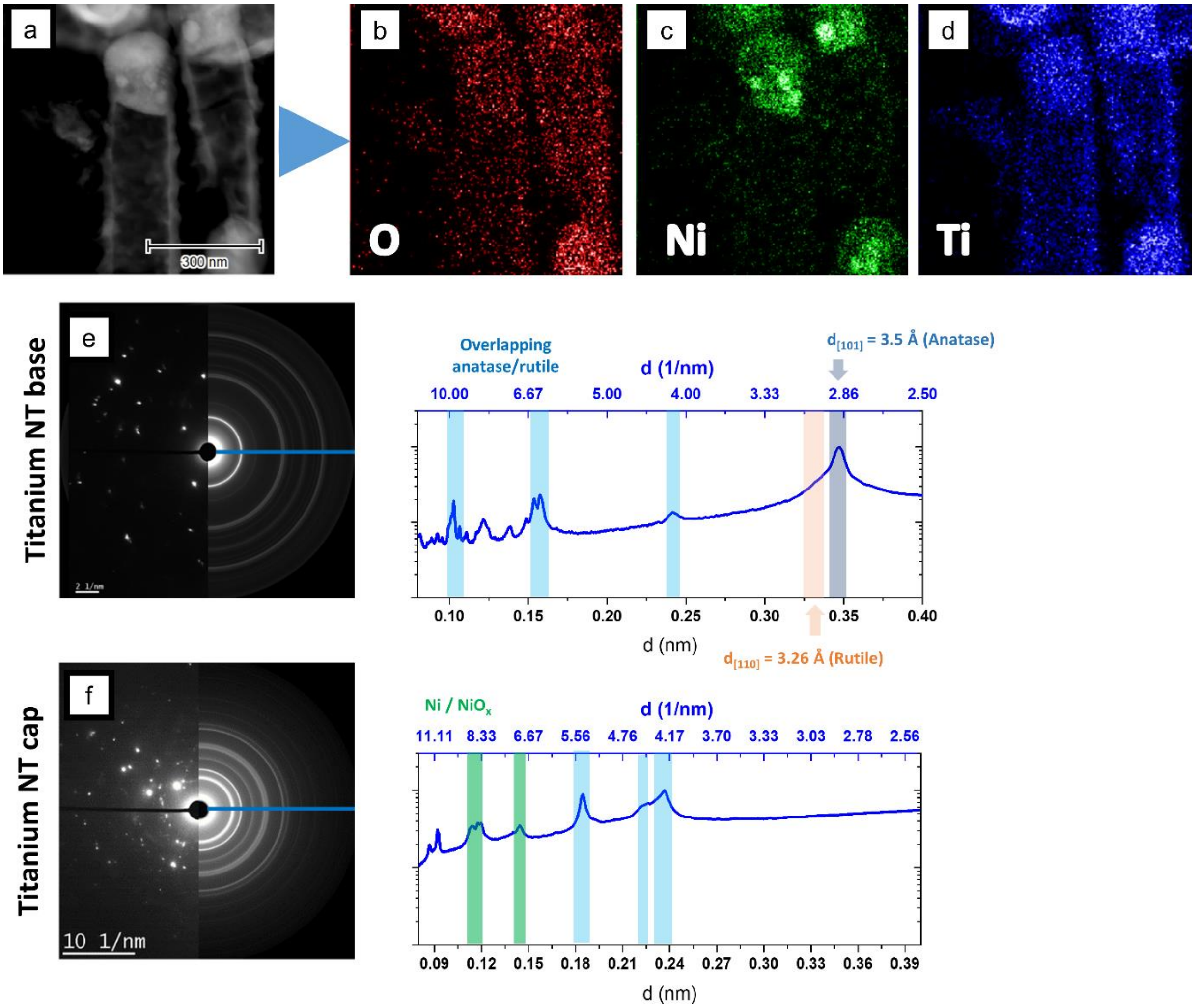

Figure S2: TEM image of the side of the nanotube irradiated with 50 mJ cm^{-2} (a), the EDX map revealing positions of O (b), Ni (c), and Ti (d). The SAED pattern and radial reconstruction[1] of the NiO$_2$NT base (e) and cap (f), as well as their interpretation according to the respective intensity profiles.

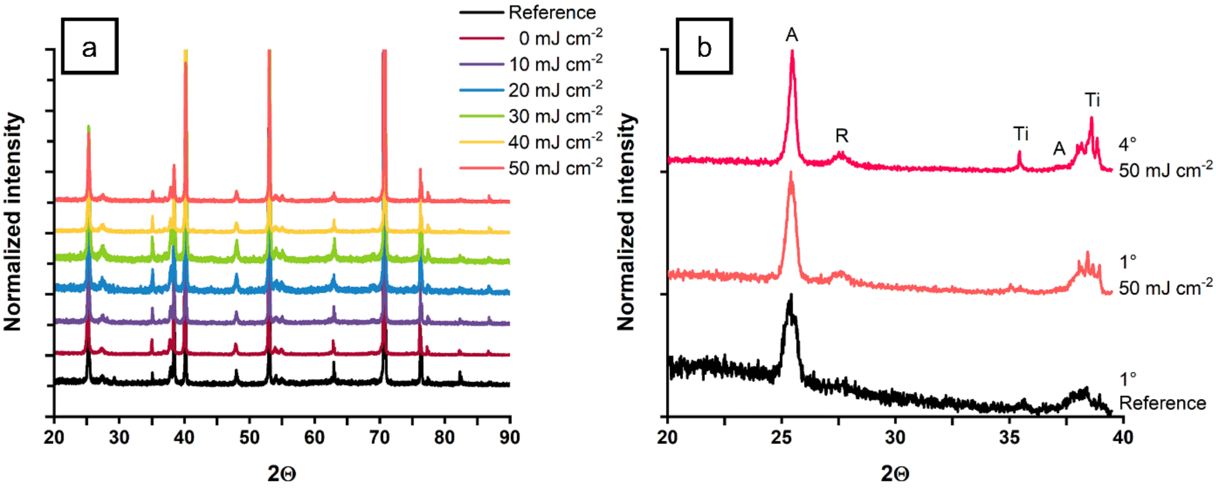

Figure S3: XRD patterns of the investigated samples obtained with θ-θ (a) and grazing-incidence scan (b).

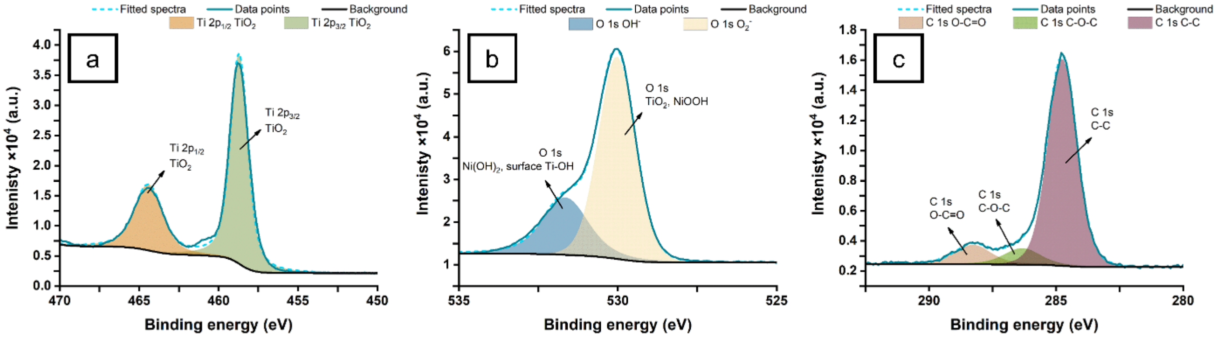

Figure S4: Deconvoluted XPS spectra within the Ti (a), O (b), and C (c) range.

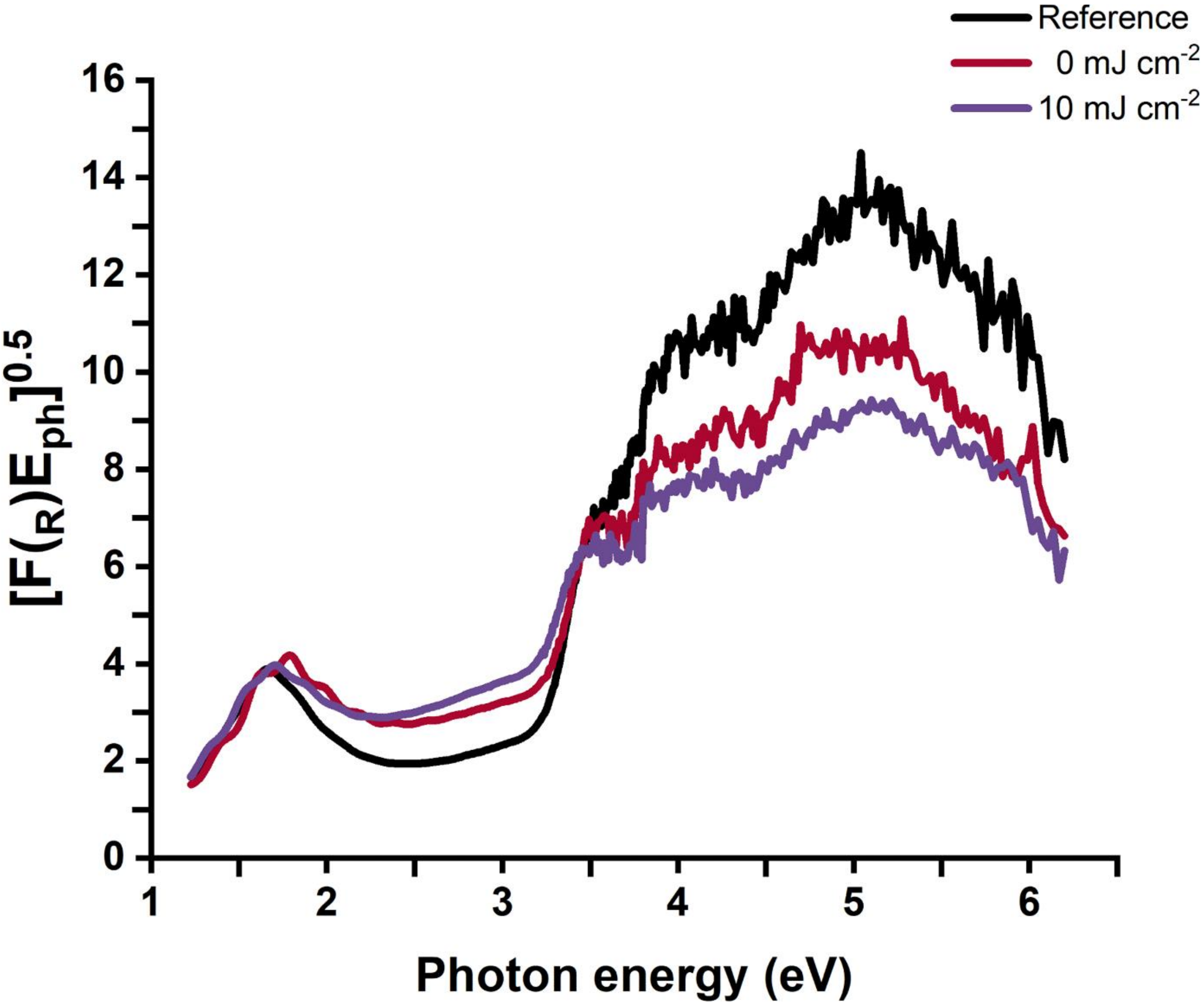

Figure S5: Calculated Tauc plots for samples that exhibited optical electron bandgap.

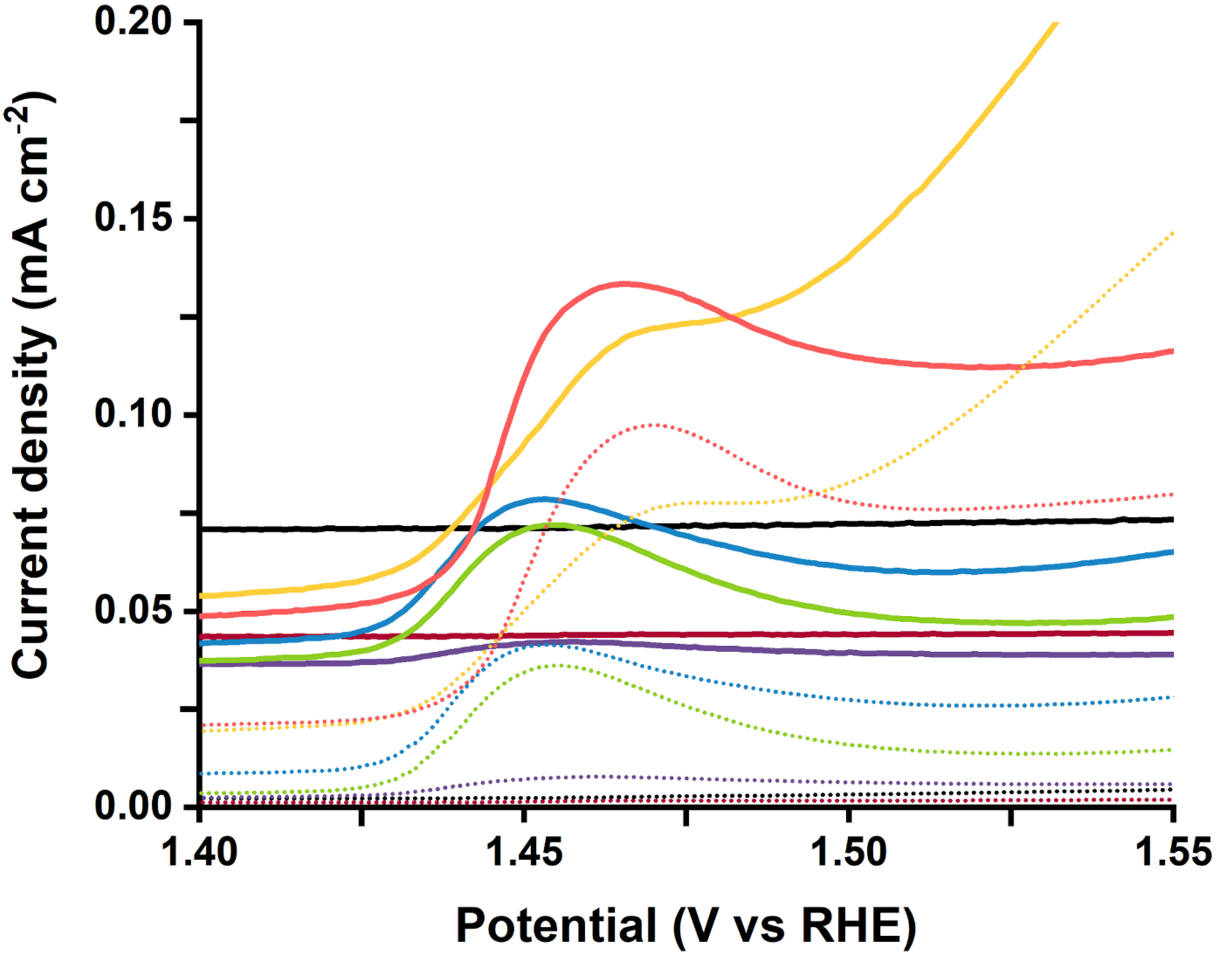

Figure S6: Close-up of Figure 3a.

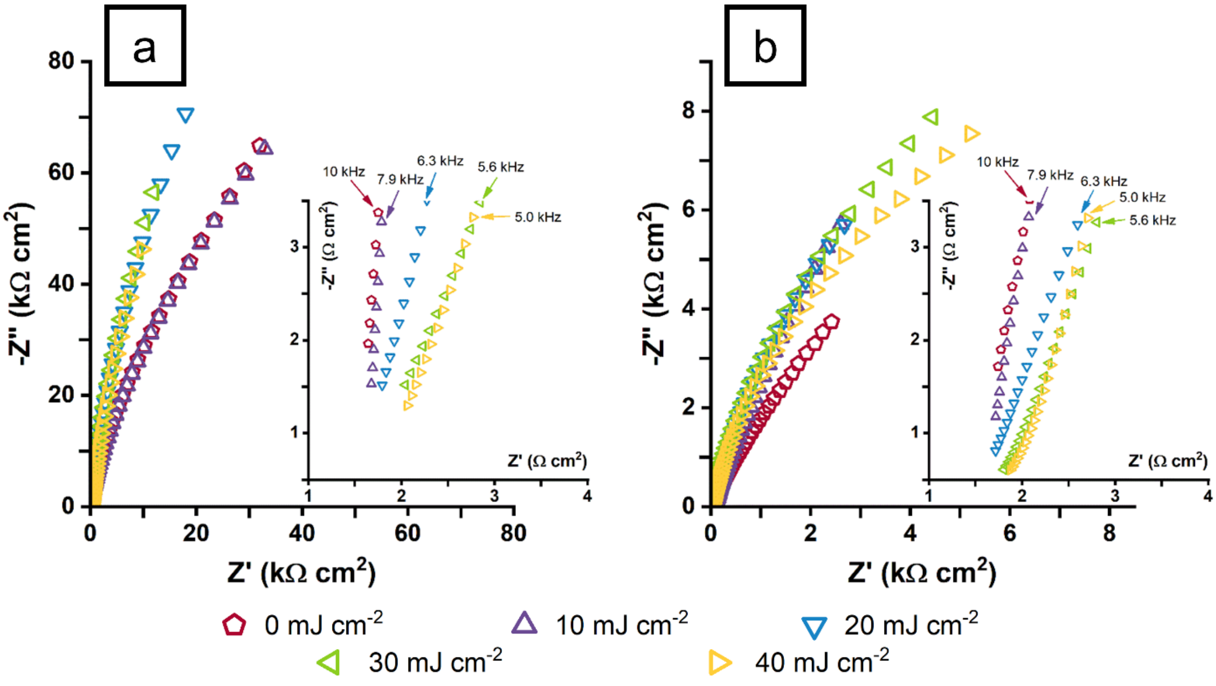

Figure S7: Nyquist plots of the laser-modified samples in dark (a) and under simulated solar radiation (b).

Table S8: Comparison of current advances in water-splitting technologies.

Electrode material	Electrolyte	Overpotential η	Ref.
Ni@TiO_2NTs	**0.5 M NaOH**	**420 mV @ 10 mA cm^{-2}**	**This work**
Ni-TiO_2	0.1 M KOH	470 mV @ 10 mA cm^{-2}	[2]
Ni-TiO_2	0.1 M KOH	550 mV @ 0.5 mA cm^{-2}	[3]
Co-TiO_2	0.1 M KOH	620 mV @ 10 mA cm^{-2}	[3]
$NiTiO_2$	0.1 M KOH	450 mV @ 0.5 mA cm^{-2}	[4]
MnO_2@TiO_2NTs	0.1 M KOH	665 mV @ 10 mA cm^{-2}	[5]
IrO_2@TiO_2NTs	0.5 M H_2SO_4	750 mV @ 0.5 mA cm^{-2}	[6]
TiO_2:CoO.03 NWs	1 M KOH	720 mV @ 10 mA cm^{-2}	[7]
Blue TiO_2 NTs	KH_2PO_4 with NaOH (pH = 7.2)	1800 mV @ 10 mA cm^{-2}	[8]
Black TiO_2NTs	KH_2PO_4 with NaOH (pH = 7.2)	1200 mV @ 10 mA cm^{-2}	[8]
Co(OH)x/Ti	1 M KOH	434 mV @ 10 mA cm^{-2}	[9]
CoOx/black TiO_2NTs	1 M KOH	352 mV @ 10 mA cm^{-2}	[9]
Ni-TiO_2	0.1 M KOH	430 mV @6 mA cm^{-2}	[4]
Ni-ZIF/Ni-B	1 M KOH	234 mV @ 10 mA cm^{-2}	[10]
$NiCoO_4$ NWs	1 M KOH	420 mV@ 5 mA cm^{-2}	[11]
FeOx, FeSx, Fe	0.1 M KOH	450 mV @ 10 mA cm^{-2}	[12]
Ni	0.1 M KOH	517 mV @ 10 mA cm^{-2}	[13]
Ni-exsolved $CaTiO_3$	0.1 M KOH	568 mV @10 mA cm^{-2}	[13]

Table S9: The electrical parameters obtained from fitting procedure based on EQC given in Fig. 3f for reference and laser treated titania with 50 mJ cm^{-2}.

Element	Reference	Laser treated	Element	Reference	Laser treated
R_e (Ω cm^{-2})	1.0	1.45	CPE_1 (10^{-5} Ω^{-1} cm^{-2} s^n)	4.62	2.41
R_1 (Ω cm^{-2})	823.7	3.0	n_1	0.87	0.90
R_2 (Ω cm^{-2})	4392.4	1074	CPE_2 (10^{-6} Ω^{-1} cm^{-2} s^n)	5.3	14.8
W_{or} (Ω cm^{-2} $s^{0.5}$)	23104	8837.6	n_2	0.81	0.94
W_{oc} ($s^{0.5}$)	3.00	0.03	χ^2	10^{-5}	4.7×10^{-3}

References

[1] D. R. G. Mitchell, *Microsc. Res. Tech.*, **2008**, *71*, 588. https://doi.org/10.1002/jemt.20591.

[2] A. Guiet, T. N. Huan, C. Payen, F. Porcher, V. Mougel, M. Fontecave, G. Corbel, *ACS Appl. Mater. Interfaces*, **2019**, *11*, 31038. https://doi.org/10.1021/acsami.9b08535.

[3] D. M. Jang, I. H. Kwak, E. L. Kwon, C. S. Jung, H. S. Im, K. Park, J. Park, *J. Phys. Chem. C*, **2015**, *119*, 1921. https://doi.org/10.1021/jp511561k.

[4] R. Ramesh, S. Lee, S. Kim, J. Park, S. Lee, M. S. Kim, M. Baek, K. Yong, Y. Ye, J. Lee, *ChemistrySelect*, **2018**, *3*, 5130. https://doi.org/10.1002/slct.201800594.

[5] X. Li, M. Zhang, Y. Zhang, C. Yu, W. Qi, J. Cui, Y. Wang, Y. Qin, J. Liu, X. Shu, Y. Chen, T. Xie, Y. Wu, *Int. J. Hydrogen Energy*, **2018**, *43*, *14369*. https://doi.org/10.1016/j.ijhydene.2018.06.027.

[6] Y. Shi, Z. Lu, L. Guo, Z. Wang, C. Guo, H. Tan, C. Yan, *Int. J. Hydrogen Energy*, **2018**, *43*, 9133. https://doi.org/10.1016/j.ijhydene.2018.03.214.

[7] L. Cai, I. S. Cho, M. Logar, A. Mehta, J. He, C. H. Lee, P. M. Rao, Y. Feng, J. Wilcox, F. B. Prinz, X. Zheng, *Phys. Chem. Chem. Phys.*, **2014**, *16*, 12299. https://doi.org/10.1039/C4CP01748J.

[8] C. Kim, S. Kim, S. P. Hong, J. Lee, J. Yoon, *Phys. Chem. Chem. Phys.*, **2016**, *18*, 14370. https://doi.org/10.1039/C6CP01799A.

[9] Y. Yang, L. C. Kao, Y. Liu, K. Sun, H. Yu, J. Guo, S. Y. H. Liou, M. R. Hoffmann, *ACS Catal.*, **2018**, *8*, 4278. https://doi.org/10.1021/acscatal.7b04340.

[10] H. Xu, B. Fei, G. Cai, Y. Ha, J. Liu, H. Jia, J. Zhang, M. Liu, R. Wu, *Adv. Energy Mater.*, **2020**, *10*, 1902714. https://doi.org/10.1002/aenm.201902714.

[11] Z. Peng, D. Jia, A. M. Al-Enizi, A. A. Elzatahry, G. Zheng, *Adv. Energy Mater.*, **2015**, *5*, 1402031. https://doi.org/10.1002/aenm.201402031.

[12] B. C. M. Martindale, E. Reisner, *Adv. Energy Mater.*, **2016**, *6*, 1502095. https://doi.org/10.1002/aenm.201502095.

[13] J. G. Lee, J. Myung, A. B. Naden, O. S. Jeon, Y. G. Shul, J. T. S. Irvine, *Adv. Energy Mater.*, **2020**, *10*, 1903693. https://doi.org/10.1002/aenm.201903693.